

Experimental Observation of Non-Abelian Earring Nodal Links in Phononic Crystals

Mudi Wang¹,¹ Shan Liu,² Qiyun Ma,² Ruo-Yang Zhang^{1,*}, Dongyang Wang¹, Qinghua Guo,^{1,3}
Biao Yang,^{1,4} Manzhu Ke,² Zhengyou Liu,^{2,5,†} and C. T. Chan^{1,‡}

¹Department of Physics, The Hong Kong University of Science and Technology, Hong Kong 999077, China

²Key Laboratory of Artificial Micro- and Nanostructures of Ministry of Education and School of Physics and Technology, Wuhan University, Wuhan 430072, China

³Institute for Advanced Study, The Hong Kong University of Science and Technology, Hong Kong 999077, China

⁴College of Advanced Interdisciplinary Studies, National University of Defense Technology, Changsha 410073, China

⁵Institute for Advanced Studies, Wuhan University, Wuhan 430072, China



(Received 2 August 2021; accepted 20 April 2022; published 14 June 2022)

Nodal lines are symmetry-protected one-dimensional band degeneracies in momentum space, which can appear in numerous topological configurations such as nodal rings, chains, links, and knots. Very recently, non-Abelian topological physics have been proposed in space-time inversion (PT) symmetric systems. One of the most special configurations in such systems is the earring nodal link, composing of a nodal chain linking with an isolated nodal line. Such earring nodal links have not been observed in real systems. We designed phononic crystals with earring nodal links, and experimentally observed two different kinds of earring nodal links by measuring the band structures. We found that the order of the nodal chain and line can be switched after band inversion but their link cannot be severed. Our Letter provides experimental evidence for phenomena unique to non-Abelian band topology and our acoustic system provides a convenient platform for studying the new materials carrying non-Abelian charges.

DOI: [10.1103/PhysRevLett.128.246601](https://doi.org/10.1103/PhysRevLett.128.246601)

Topological materials, such as topological insulators [1–11], Weyl or Dirac points [12–20], and nodal line semimetals [21–30], have attracted much attention in both theory and experiment. These materials can be characterized by quantized topological invariants, that can be classified by Abelian groups Z or Z_2 . Very recently, a new type of topological classification using non-Abelian groups has been proposed for space-time inversion symmetric multiband systems [31], prompting the discovery of braiding topological structures [32–42] in non-Abelian systems.

The band structure in non-Abelian systems supports some special configurations in moment space protected by non-Abelian topological charges. One of the most interesting configurations is the earring nodal link [31], the existence and robustness of which cannot be explained by conventional Abelian topology that defines topological invariants by considering a single band gap. Such earring nodal links can be observed in a three-band system, where the non-Abelian topology can be described by a quaternion charge of “ -1 .” In this Letter, we report the first experimental observation of earring nodal links and their non-trivial evolution as the system parameter changes. We designed and fabricated three-dimensional (3D) phononic crystals and experimentally observed two kinds of earring nodal links.

In a three-band PT -symmetric system, the space of the Hamiltonian without degeneracies in the momentum space

is $M_3 = O(3)/O(1)^3$, where $O(N)$ is the N -dimensional orthogonal group. Its fundamental homotopy group is the non-Abelian quaternion group $\pi_1(M_3) = Q = \{-1, \pm i, \pm j, \pm k, +1\}$, with group elements satisfying $i^2 = j^2 = k^2 = -1$, and $ij = -ji = k$. The characteristics of the global nodal line configuration can be described by these non-Abelian topological charges. In this Letter, we focus on the quaternion charge -1 .

Let us consider a three-band 3D system. We start by constructing a triple degeneracy lying at the intersection line of two mirror-invariant planes in the momentum space. The little group of a \mathbf{k} point on the k_z axis (i.e., the intersection of two mirror-invariant planes $k_x = 0$ and $k_y = 0$) is C_{2v} . Suppose that two of the three eigenmodes on the k_z axis have opposite parities on both the x and y mirror planes, we can write the 3-by-3 representations of the two mirror operators as

$$M_x = \begin{pmatrix} -1 & 0 & 0 \\ 0 & 1 & 0 \\ 0 & 0 & 1 \end{pmatrix}, \quad M_y = \begin{pmatrix} 1 & 0 & 0 \\ 0 & -1 & 0 \\ 0 & 0 & 1 \end{pmatrix}. \quad (1)$$

Then, (see Supplemental Material [43]) the general form of the $\mathbf{k} \cdot \mathbf{p}$ Hamiltonian respecting PT and C_{2v} symmetries near the k_z axis (up to the second order of k_x, k_y) can be written as

$$H(k_x, k_y, k_z) = \begin{pmatrix} f_1(k_z, k_x^2, k_y^2) & w_{xy}k_xk_y & (v_x^0 + v_x^1k_z)k_x \\ w_{xy}k_xk_y & f_2(k_z, k_x^2, k_y^2) & (v_y^0 + v_y^1k_z)k_y \\ (v_x^0 + v_x^1k_z)k_x & (v_y^0 + v_y^1k_z)k_y & f_3(k_z, k_x^2, k_y^2) \end{pmatrix}, \quad (2)$$

where $f_i(k_z, k_x^2, k_y^2) = g_i(k_z) + \sum_{j=x,y} k_j^2 h_{ij}(k_z)$ ($j = 1, 2, 3$), w and v are arbitrary real numbers. A threefold degeneracy along the k_z axis requires $g_1(k_z) = g_2(k_z) = g_3(k_z)$, which can appear accidentally with some specific system parameters. As an example, we consider a specific Hamiltonian

$$H_1(k_x, k_y, k_z) = \begin{pmatrix} k_z & 0.5k_xk_y & 1.5k_x \\ 0.5k_xk_y & 0.3k_z + b & (1 - 0.2k_z)k_y \\ 1.5k_x & (1 - 0.2k_z)k_y & 0 \end{pmatrix}, \quad (3)$$

which is a special case of H in Eq. (2). The distribution of the nodal lines of H_1 is shown in Fig. 1(a). There is a triple point at $k_z = 0$ plane when $b = 0$, and the Hamiltonian (up to first order and a frequency shift) in the transverse plane of $k_z = 0$ will reduce to

$$H_1(k_x, k_y, k_z = 0) = v_x^0 k_x \hat{\lambda}_2 + v_y^0 k_y \hat{\lambda}_3 = \begin{pmatrix} 0 & 0 & v_x^0 k_x \\ 0 & 0 & v_y^0 k_y \\ v_x^0 k_x & v_y^0 k_y & 0 \end{pmatrix}. \quad (4)$$

Here, $\hat{\lambda}_i$ denote the Gell-Mann matrices, and $\hat{\lambda}_2, \hat{\lambda}_3, \hat{\lambda}_4$ satisfy the angular momentum commutation relation $[\hat{\lambda}_i, \hat{\lambda}_j] = i\epsilon_{ijk}\hat{\lambda}_k$ ($i, j = 2, 3, 4, i \neq j$). As such, they form a representation of spin-one operators $\hat{\lambda}_2 = \hat{S}_x$, $\hat{\lambda}_3 = \hat{S}_y$, and $\hat{\lambda}_4 = \hat{S}_z$. The transverse Hamiltonian at the accidental triple point, with the band dispersion shown in Fig. 1(d), is in fact the two-dimensional (2D) spin-one Hamiltonian of a Dirac-like cone [44,47–57] (see Supplemental Material [43]) that has been studied widely as an effectively zero-refractive-index system. When the wave vector winds around the triple point one time along the green loop in Fig. 1(a), the generalized argument $\phi = \arg(v_x^0 k_x + i v_y^0 k_y)$ also changes 2π [43]. As a result, the triple point behaves as a topological defect of the orthonormal frame formed by the eigenvectors of the three bands, around which the frame of eigenvectors rotates one turn about the z axis as shown by the distribution of eigenvectors in Fig. 1(e). The three color bars at each point in Fig. 1(e) denote the three orthogonal real-valued eigenvectors at that point. Therefore, we have demonstrated that the spin-one Hamiltonian corresponds to 2π rotation of all three eigenstates about the fixed axis (z axis), and this eigenstate frame rotation is the key feature of the non-Abelian quaternion charge -1 [31], as shown in Fig. 1(f) which shows the rotation of the eigenstates frame on the unit sphere along the green loop in Fig. 1(a). From the Abelian topological viewpoint, the 2D spin-one triple point in Fig. 1(d) is entirely accidental and has no topological protection because the Berry phase around the triple point of every band is zero [55–57]. From a multiple band viewpoint, the 2D spin-one triple point is protected by the conservation of the quaternion charge -1 characterized by the winding of eigenstates around the triple point. This explains why the degeneracies between the three bands forming the Dirac-like cone in 2D PT -symmetric crystals can never be fully gapped and their evolution is governed by the non-Abelian charge (See Figs. S1 and S2 [43]).

The above analysis indicates that this triple degenerate point as the crossing point of the two nodal lines in Fig. 1(a), is protected by the conservation of nontrivial quaternion charge -1 . These two nodal lines have to be linked together in some way and cannot be completely separated by tuning the system parameters. As shown in Fig. 1(b), when b is changed to 0.15, a new nodal ring (red circle) of the lower two bands appears between the two nodal lines, which forms a nodal link with the blue nodal line and forms a nodal chain with the red nodal line. The underlying

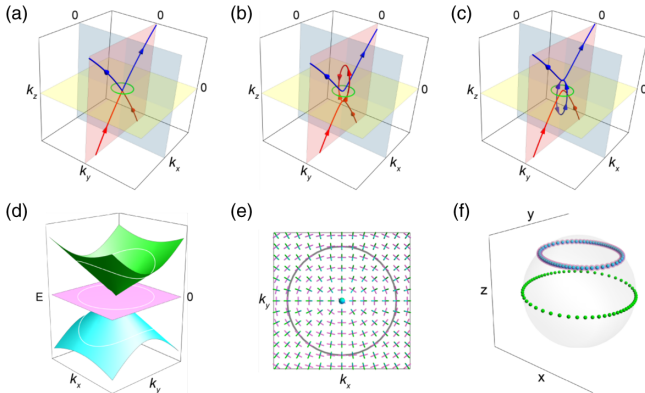


FIG. 1. (a) Nontrivial accidental triple degeneracy in momentum space. The red (blue) nodal lines are formed by the lower (upper) pair of bands. (b),(c) The two earring nodal link configurations when two different perturbations (changing the value of b from 0 to 0.15 and -0.15 , respectively) are added to the case of the nontrivial accidental triple degeneracy. (d) The dispersion at $k_z = 0$ for (a). (e) Eigenstates on the $k_z = 0$ plane, where the three color bars represent the three orthogonal eigenstates and the gray circle corresponds to the green loop in (a). (f) The rotation of the eigenstates frame on the unit sphere along green loop in (a), where the spheres with the same color trace out the trajectory of the eigenstates of each band. In (d)–(f), cyan, light magenta, and green colors correspond to bands 1, 2, and 3, respectively.

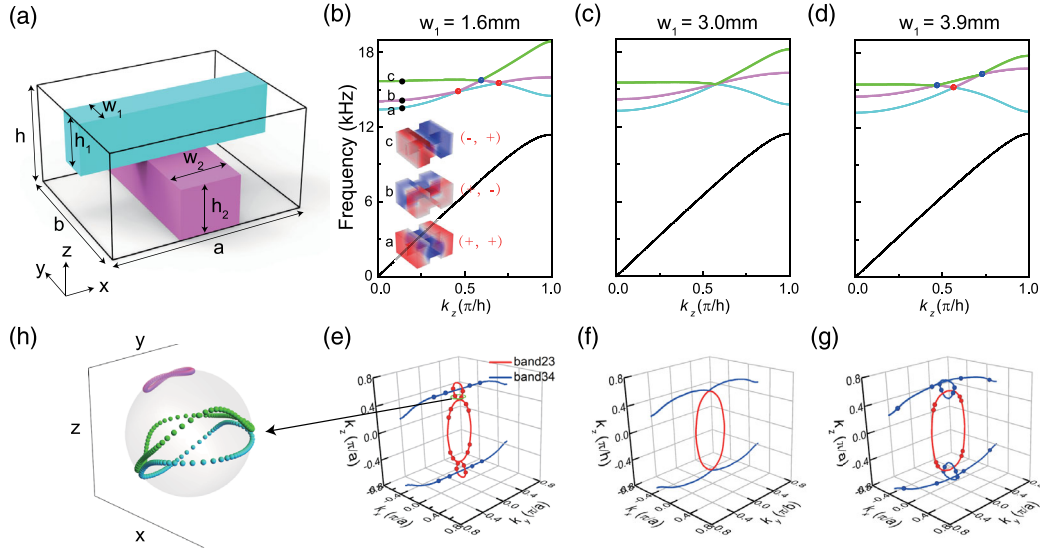


FIG. 2. (a) The unit cell of the phononic crystals. (b)–(d) The corresponding band structures along k_z with $w_1 = 1.6, 3.0,$ and 3.9 mm. $(+, +)$ indicates that the sound pressure field of the eigenmode is even in both the x and y directions at the intersection of the two mirror planes $k_x = k_y = 0$. $(+, -)$ indicates that the pressure field is an even mode in the x direction and an odd mode in the y direction, and $(-, +)$ indicates that the pressure field is an odd mode in the x direction and an even mode in the y direction. The black dots mark three eigenstates in bands 2–4 with different symmetries, and the distribution of the pressure fields is shown in the illustration. The red (blue) dots represent the nodal points of band 23 (band 34). (e)–(g) The distribution of nodal lines in (e)–(g) corresponding to the band structures in (b)–(d), respectively. The red and blue dots in (e)–(g) correspond to the red and blue nodal points in Figs. 3(b)–3(d) [Figs. 3(f)–3(h)]. (h) The rotation of the eigenstate frame on the unit sphere along green loop at $k_z = 0.5\pi/h$ in full-wave simulations.

mechanism is that the nontrivial non-Abelian quaternion charge -1 cannot be changed by small perturbations, so the green loop in Fig. 1(b) must encircle at least two nodal lines with the same orientation of the same pair of bands, which ensures the existence of a nodal ring between the two nodal lines. When a different perturbation is applied, such as changing b to -0.15 , another configuration of the earring nodal link appears, as shown in Fig. 1(c). The newly emerging blue nodal ring of the upper two bands and the blue line form a nodal chain, while the blue nodal ring and red nodal line form a nodal link. These hybrid configurations of a nodal link and nodal chain, called earring nodal links [31], can be understood using non-Abelian topology and cannot be explained by Abelian topology.

To experimentally observe the earring nodal links similar to those shown in Figs. 1(b) and 1(c), we designed a cubic layer-by-layer phononic crystal with a unit cell consisting of two stacked cuboids with different sizes that are twisted by $\pi/2$ along the z direction. The sample has two mirror symmetries and inversion symmetry, which are the necessary conditions to construct the earring nodal links in k space. The space group is $Pmmm$. The unit cell is shown in Fig. 2(a), and the structural parameters are $a = 22.6$ mm, $b = 18.8$ mm, $w_2 = 7.1$ mm, $h_1 = 6$ mm, $h_2 = 6$ mm, and $h = 12$ mm. Our full-wave simulations are performed using COMSOL Multiphysics. As this structure has mirror symmetries in both the x and y directions, each mode has well-defined mirror parity in the corresponding mirror

planes. The simulated dispersion curves along the k_z direction with $w_1 = 1.6$ mm are shown in Fig. 2(b), and the pressure field distributions for the eigenstates in bands 2–4 have three different mode symmetries $(+, +)$, $(+, -)$, and $(-, +)$ as indicated in the figure. The three bands intersect each other, and the red (blue) points represent the nodal points of the two lower (higher) bands. Since the little group of a general k point on the k_z axis is C_{2v} , and these three bands satisfy the representation given in Eq. (1), the dispersion can be captured faithfully by the model Hamiltonian in Eq. (2) which gives the $k \cdot p$ Hamiltonian for the three bands near the k_z axis. When w_1 is increased to 3.0 mm, bands 2–4 become accidentally degenerate at one point, as shown in Fig. 2(c). Increasing w_1 to 3.9 mm, bands 2–4 will intersect each other again. The nodal lines in k space are found numerically and are shown in Figs. 2(e)–2(g) (solid lines). They have the same features as the model Hamiltonian shown in Figs. 1(a)–1(c). We verify the non-Abelian topological charge in the full-wave simulations (see Supplemental Material [43]), and the effective eigenstate frames obtained along the loop are plotted on the unit sphere in Fig. 2(h). This shows the 2π rotation of all three eigenstates on the unit sphere about the z axis, which confirms that the earring nodal link in the real phononic crystal is protected by a quaternion charge -1 .

Using 3D printing, we fabricated an experimental sample containing $21 \times 21 \times 21$ unit cells, as shown in Fig. 3(a). The sample has the same symmetry as the Hamiltonian H_1

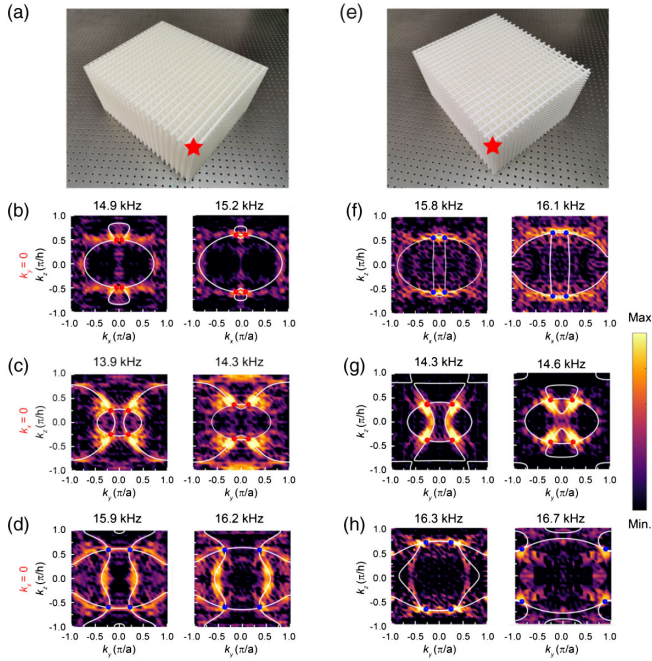


FIG. 3. (a) Experimental sample-1 [the structural parameters are the same as in Fig. 2(e)]. The red star is the position of the point source. (b)–(d) Experimental (color maps) and theoretical (white lines) equal-frequency contours at $k_y = 0$ and $k_x = 0$ for different frequencies for sample 1. The theoretical nodal points are marked by red or blue dots. (e) Experimental sample 2 [the structural parameters are the same as in Fig. 2(g)]. (f)–(g) Experimental and theoretical band structures at $k_y = 0$ and $k_x = 0$ for different frequencies for sample 2. The theoretical nodal points are marked by red or blue dots.

and exhibits the earring nodal links as shown in Fig. 2(e). We place an acoustic point source at the position of the red star. We insert a movable microphone (diameter ~ 0.7 cm, B&K Type 4187) into the sample through the interstitial voids to scan the acoustic field of the whole sample. The band dispersions on the planes of $k_x = 0$ and of $k_y = 0$ at different frequencies are obtained experimentally by performing 3D Fourier transforms of the scanned fields, and are compared with numerically computed equal-frequency contours (white lines), as shown in Figs. 3(b)–3(d). At each frequency, four theoretical nodal points are marked in red or blue, helping us to find the nodal points from the experimental data which are located at the intersections of equal-frequency contours. The nodal points in Fig. 3(b) correspond to the red dots in Fig. 2(e) at the $k_y = 0$ plane. The nodal points in Figs. 3(c) and 3(d) correspond to the red and blue dots in Fig. 2(e) at the $k_x = 0$ plane, respectively. Hence, the nodal links with earring shape are verified experimentally.

To demonstrate the exotic evolution of the earring nodal link protected by the conservation of the non-Abelian -1 charge, another sample [Fig. 3(e)] with $w_1 = 3.9$ mm corresponding to Fig. 2(g) was fabricated. The band

dispersions obtained using the Fourier transform of the scanned fields are shown in Figs. 3(f)–3(h) for different frequencies, and we can see the position of the nodal point with the help of the theoretical result. Hence, the other configuration of earring nodal links, whose existence is protected by the quaternion charge -1 , is also observed in experiment.

In summary, we showed theoretically that the triple point characterized by a 2D spin-one Hamiltonian is related to the non-Abelian quaternion charge -1 in a 3D system, which shows that the horizon of topological protection can be broadened if we extend the scope from Abelian to non-Abelian and also contributes to the understanding of the spin-one conical diffraction effect [45,46] (see Supplemental Material [43]). We also revealed that indestructible earring nodal links can emerge from the perturbation of the triple point, and we numerically verified the non-Abelian topological charge -1 carried by nodal link from full-wave simulations. Moreover, we experimentally observed earring nodal links, and the earring nodal links before and after band inversion are measured at two system configurations, providing evidence for the nontrivial evolution of the earring nodal link and experimentally manifesting the stability of the quaternion charge -1 . Our results provide an experimental basis for the theory of non-Abelian band topology and offer a simple three-dimensional acoustic system as a platform to explore new phenomena associated with multiband topology.

This work is supported by Hong Kong RGC Grant No. AoE/P-502/20, Grant No. 16307821, KAUST CRG grant (KAUST20SC01), the Croucher foundation (CAS20SC01), the National Key R&D Program of China (Grant No. 2018YFA0305800), and the National Natural Science Foundation of China (Grants No. 11890701, No. 11774275 and No. 11974262).

* ruoyangzhang@ust.hk

† zyliu@whu.edu.cn

‡ phchan@ust.hk

- [1] M. Z. Hasan and C. L. Kane, Colloquium: Topological insulators, *Rev. Mod. Phys.* **82**, 3045 (2010).
- [2] X. L. Qi and S. C. Zhang, Topological insulators and superconductors, *Rev. Mod. Phys.* **83**, 1057 (2011).
- [3] A. B. Khanikaev, S. H. Mousavi, W.-K. Tse, M. Kargarian, A. H. MacDonald, and G. Shvets, Photonic topological insulators, *Nat. Mater.* **12**, 233 (2013).
- [4] L. Lu, J. D. Joannopoulos, and M. Soljacic, Topological photonics, *Nat. Photonics* **8**, 821 (2014).
- [5] Z. Yang, F. Gao, X. Shi, X. Lin, Z. Gao, Y. Chong, and B. Zhang, Topological Acoustics, *Phys. Rev. Lett.* **114**, 114301 (2015).
- [6] C. He, X. Ni, H. Ge, X.-C. Sun, Y.-B. Chen, M.-H. Lu, X.-P. Liu, and Y.-F. Chen, Acoustic topological insulator and robust one-way sound transport, *Nat. Phys.* **12**, 1124 (2016).

- [7] J. Lu, C. Qiu, L. Ye, X. Fan, M. Ke, F. Zhang, and Z. Liu, Observation of topological valley transport of sound in sonic crystals, *Nat. Phys.* **13**, 369 (2017).
- [8] G. Harari, M. A. Bandres, Y. Lumer, M. C. Rechtsman, Y. D. Chong, M. Khajavikhan, D. N. Christodoulides, and M. Segev, Topological insulator laser: Theory, *Science* **359**, eaar4003 (2018).
- [9] M. A. Bandres, S. Wittek, G. Harari, M. Parto, J. Ren, M. Segev, D. N. Christodoulides, and M. Khajavikhan, Topological insulator laser: Experiments, *Science* **359**, eaar4005 (2018).
- [10] H. Xue, Y. Yang, F. Gao, Y. Chong, and B. Zhang, Acoustic higher-order topological insulator on a kagome lattice, *Nat. Mater.* **18**, 108 (2019).
- [11] M. Wang, W. Zhou, L. Bi, C. Qiu, M. Ke, and Z. Liu, Valley-locked waveguide transport in acoustic heterostructures, *Nat. Commun.* **11**, 1 (2020).
- [12] L. Lu, Z. Wang, D. Ye, L. Ran, L. Fu, J. D. Joannopoulos, and M. Soljačić, Experimental observation of Weyl points, *Science* **349**, 622 (2015).
- [13] B. Yang, Q. Guo, B. Tremain *et al.*, Direct observation of topological surface-state arcs in photonic metamaterials, *Nat. Commun.* **8**, 1 (2017).
- [14] N. P. Armitage, E. J. Mele, and A. Vishwanath, Weyl and Dirac semimetals in three-dimensional solids, *Rev. Mod. Phys.* **90**, 015001 (2018).
- [15] H. He, C. Qiu, L. Ye, X. Cai, X. Fan, M. Ke, F. Zhang, and Z. Liu, Topological negative refraction of surface acoustic waves in a Weyl phononic crystal, *Nature (London)* **560**, 61 (2018).
- [16] B. Yang *et al.*, Ideal Weyl points and helicoid surface states in artificial photonic crystal structures, *Science* **359**, 1013 (2018).
- [17] F. Li, X. Huang, J. Lu, J. Ma, and Z. Liu, Weyl points and Fermi arcs in a chiral phononic crystal, *Nat. Phys.* **14**, 30 (2018).
- [18] D. Wang, B. Yang, W. Gao *et al.*, Photonic Weyl points due to broken time-reversal symmetry in magnetized semiconductor, *Nat. Phys.* **15**, 1150 (2019).
- [19] B. J. Wieder, Z. Wang, J. Cano, X. Dai, L. M. Schoop, B. Bradlyn, and B. A. Bernevig, Strong and fragile topological Dirac semimetals with higher-order Fermi arcs, *Nat. Commun.* **11**, 627 (2020).
- [20] H.-X. Wang, Z.-K. Lin, B. Jiang, G.-Y. Guo and J.-H. Jiang, Higher-Order Weyl Semimetals, *Phys. Rev. Lett.* **125**, 146401 (2020).
- [21] A. A. Burkov, M. D. Hook, and L. Balents, Topological nodal semimetals, *Phys. Rev. B* **84**, 235126 (2011).
- [22] T. Bzdušek, Q. S. Wu, A. Rüegg, M. Sigrist, and A. A. Soluyanov, Nodal-chain metals, *Nature (London)* **538**, 75 (2016).
- [23] C. Fang, H. Weng, X. Dai, and Z. Fang, Topological nodal line semimetals, *Chin. Phys. B* **25**, 117106 (2016).
- [24] Q. Yan, R. Liu, Z. Yan, B. Liu, H. Chen, Z. Wang, and L. Lu, Experimental discovery of nodal chains, *Nat. Phys.* **14**, 461 (2018).
- [25] W. Gao, B. Yang, B. Tremain, H. Liu, Q. Guo, L. Xia, A. P. Hibbins, and S. Zhang, Experimental observation of photonic nodal line degeneracies in metacrystals, *Nat. Commun.* **9**, 1 (2018).
- [26] W. Deng, J. Lu, F. Li, X. Huang, M. Yan, J. Ma, and Z. Liu, Nodal rings and drumhead surface states in phononic crystals, *Nat. Commun.* **10**, 1769 (2019).
- [27] Z.-G. Geng, Y.-G. Peng, Y.-X. Shen, Z. Ma, R. Yu, J.-H. Gao, and X.-F. Zhu, Topological nodal line states in three-dimensional ball-and-stick sonic crystals, *Phys. Rev. B* **100**, 224105 (2019).
- [28] Y. Yang, J. Xia, H. Sun, Y. Ge, D. Jia, S. Yuan, S. Yang, Y. Chong, and B. Zhang, Observation of a topological nodal surface and its surface-state arcs in an artificial acoustic crystal, *Nat. Commun.* **10**, 1 (2019).
- [29] A. Merkel and J. Christensen, Ultrasonic nodal chains in topological granular metamaterials, *Commun. Phys.* **2**, 154 (2019).
- [30] J. Lu, X. Huang, M. Yan, F. Li, W. Deng, and Z. Liu, Nodal-Chain Semimetal States and Topological Focusing in Phononic Crystals, *Phys. Rev. Applied* **13**, 054080 (2020).
- [31] Q. S. Wu, A. A. Soluyanov, and T. Bzdušek, Non-Abelian band topology in noninteracting metals, *Science* **365**, 1273 (2019).
- [32] P. M. Lenggenhager, X. Liu, S. S. Tsirkin, T. Neupert, and T. Bzdušek, From triple-point materials to multiband nodal links, *Phys. Rev. B* **103**, L121101 (2021).
- [33] A. Tiwari and T. Bzdušek, Non-Abelian topology of nodal-line rings in PT -symmetric systems, *Phys. Rev. B* **101**, 195130 (2020).
- [34] A. Bouhon, Q. S. Wu, R. J. Slager, H. Weng, O. V. Yazyev, and T. Bzdušek, Non-Abelian reciprocal braiding of Weyl points and its manifestation in ZrTe, *Nat. Phys.* **16**, 1137 (2020).
- [35] E. Yang, B. Yang, O. You, H.-C. Chan, P. Mao, Q. Guo, S. Ma, L. Xia, D. Fan, Y. Xiang, and S. Zhang, Observation of Non-Abelian Nodal Links in Photonics, *Phys. Rev. Lett.* **125**, 033901 (2020).
- [36] F. N. Ünal, A. Bouhon, and R. J. Slager, Topological Euler Class as a Dynamical Observable in Optical Lattices, *Phys. Rev. Lett.* **125**, 053601 (2020).
- [37] A. Bouhon, T. Bzdušek, and R. J. Slager, Geometric approach to fragile topology beyond symmetry indicators, *Phys. Rev. B* **102**, 115135 (2020).
- [38] Q. Guo, T. Jiang, R.-Y. Zhang, L. Zhang, Z.-Q. Zhang, B. Yang, S. Zhang, and C. T. Chan, Experimental observation of non-Abelian topological charges and edge states, *Nature (London)* **594**, 195 (2021).
- [39] D. Wang, B. Yang, Q. Guo, R.-Y. Zhang, L. Xia, X. Su, W.-J. Chen, J. Han, S. Zhang, and C. T. Chan, Intrinsic in-plane nodal chain and generalized quaternion charge protected nodal link in photonics, *Light Sci. Appl.* **10**, 83 (2021).
- [40] H. Park, S. Wong, X. Zhang, and S. S. Oh, Non-Abelian charged nodal links in dielectric photonic crystal, *ACS Photonics* **8**, 2746 (2021).
- [41] B. Jiang, A. Bouhon, Z. K. Lin, X. Zhou, B. Hou, F. Li, R.-J. Slager, and J.-H. Jiang, Observation of non-Abelian topological semimetals and their phase transitions, *Nat. Phys.* **17**, 1239 (2021).
- [42] B. Peng, A. Bouhon, B. Monserrat, and R.-J. Slager, Non-Abelian braiding of phonons in layered silicates, *Nat. Commun.* **13**, 423 (2022).

- [43] See Supplemental Material at <http://link.aps.org/supplemental/10.1103/PhysRevLett.128.246601> for simulation and experimental measurement methods, derivation about the $\mathbf{k} \cdot \mathbf{p}$ Hamiltonian and evolution of the nodal points on 2D sections which includes Refs. [23,31,34,38,44–46].
- [44] A. Fang, Z. Q. Zhang, S. G. Louie, and C. T. Chan, Klein tunneling and supercollimation of pseudospin-1 electromagnetic waves, *Phys. Rev. B* **93**, 035422 (2016).
- [45] F. Diebel, D. Leykam, S. Kroesen, C. Denz, and A. S. Desyatnikov, Conical Diffraction and Composite Lieb Bosons in Photonic Lattices, *Phys. Rev. Lett.* **116**, 183902 (2016).
- [46] Z. Xiong, R.-Y. Zhang, R. Yu, C. T. Chan, and Y. Chen, Hidden-symmetry-enforced nexus points of nodal lines in layer-stacked dielectric photonic crystals, *Light Sci. Appl.* **9**, 1 (2020).
- [47] R. Shen, L. B. Shao, B. Wang, and D. Y. Xing, Single Dirac cone with a flat band touching on line-centered-square optical lattices, *Phys. Rev. B* **81**, 041410(R) (2010).
- [48] C.-H. Park, L. Yang, Y.-W. Son, M. L. Cohen, and S. G. Louie, Anisotropic behaviours of massless Dirac fermions in graphene under periodic potentials, *Nat. Phys.* **4**, 213 (2008).
- [49] C. Park, Y. Son, L. Yang, M. L. Cohen, and S. G. Louie, Electron beam supercollimation in graphene superlattices, *Nano Lett.* **8**, 2920 (2008).
- [50] A. A. Asatryan, L. C. Botten, M. A. Byrne, V. D. Freilikher, S. A. Gredeskul, I. V. Shadrivov, R. C. McPhedran, and Y. S. Kivshar, Suppression of Anderson Localization in Disordered Metamaterials, *Phys. Rev. Lett.* **99**, 193902 (2007).
- [51] S. K. Choi, C.-H. Park, and S. G. Louie, Electron Supercollimation in Graphene and Dirac Fermion Materials Using One-Dimensional Disorder Potentials, *Phys. Rev. Lett.* **113**, 026802 (2014).
- [52] P. Hsieh, C. Chung, J. F. McMillan, M. Tsai, M. Lu, N. C. Panoiu, and C. W. Wong, Photon transport enhanced by transverse Anderson localization in disordered superlattices, *Nat. Phys.* **11**, 268 (2015).
- [53] P. Moitra, Y. Yang, Z. Anderson, I. I. Kravchenko, D. P. Briggs, and J. Valentine, Realization of an all-dielectric zero-index optical metamaterial, *Nat. Photonics* **7**, 791 (2013).
- [54] Y. Li, S. Kita, P. Muñoz, O. Reshef, D. I. Vulis, M. Yin, M. Lončar, and E. Mazur, On-chip zero-index metamaterials, *Nat. Photonics* **9**, 738 (2015).
- [55] X. Huang, Y. Lai, Z. Hang, H. Zheng, and C. T. Chan, Dirac cones induced by accidental degeneracy in photonic crystals and zero-refractive-index materials, *Nat. Mater.* **10**, 582 (2011).
- [56] J. Mei, Y. Wu, C. T. Chan, and Z.-Q. Zhang, First-principles study of Dirac and Dirac-like cones in phononic and photonic crystals, *Phys. Rev. B* **86**, 035141 (2012).
- [57] A. Fang, Z. Q. Zhang, S. G. Louie *et al.*, Pseudospin-1 physics of photonic crystals, *Research* **2019**, 3054062 (2019).